

---

# Symplectic Adjoint Method for Exact Gradient of Neural ODE with Minimal Memory

---

**Takashi Matsubara**

Osaka University

Osaka, Japan 560-8531

[matsubara@sys.es.osaka-u.ac.jp](mailto:matsubara@sys.es.osaka-u.ac.jp)

**Yuto Miyatake**

Osaka University

Osaka, Japan 560-0043

[miyatake@cas.cmc.osaka-u.ac.jp](mailto:miyatake@cas.cmc.osaka-u.ac.jp)

**Takaharu Yaguchi**

Kobe University

Kobe, Japan 657-8501

[yaguchi@pearl.kobe-u.ac.jp](mailto:yaguchi@pearl.kobe-u.ac.jp)

## Abstract

A neural network model of a differential equation, namely neural ODE, has enabled us to learn continuous-time dynamical systems and probabilistic distributions with a high accuracy. It uses the same network repeatedly during a numerical integration. Hence, the backpropagation algorithm requires a memory footprint proportional to the number of uses *times* the network size. This is true even if a checkpointing scheme divides the computational graph into sub-graphs. Otherwise, the adjoint method obtains a gradient by a numerical integration backward in time with a minimal memory footprint; however, it suffers from numerical errors. This study proposes the symplectic adjoint method, which obtains the exact gradient (up to rounding error) with a footprint proportional to the number of uses *plus* the network size. The experimental results demonstrate the symplectic adjoint method occupies the smallest footprint in most cases, functions faster in some cases, and is robust to a rounding error among competitive methods.

## 1 Introduction

Deep neural networks have provided remarkable methods for various tasks such as image recognition [17] and natural language processing [3]. These methods employed a residual architecture [18, 28], where the output  $x_{n+1}$  of the  $n$ -th operation is defined as a subroutine  $f_n$  plus the input  $x_n$  as  $x_{n+1} = f_n(x_n) + x_n$ . The residual architecture can be viewed as a numerical integration applied to an ordinary differential equation (ODE) [25]. Accordingly, a neural network model of differential equation  $dx/dt = f(x)$ , namely neural ODE, was proposed [1]. Given an input as an initial condition  $x(0) = x_0$ , Neural ODE solves an initial value problem by a numerical integration, obtaining an output  $y = x(T)$ . Neural ODE is available for modeling a continuous-time dynamics; irregularly sampled time series [21], stable dynamical systems [30, 35], and physical phenomena associated with geometric structures [2, 12, 26]. Moreover, since neural ODE approximates a diffeomorphism [36], it is available also for modeling probabilistic distributions of real-world data by the change of variables [11, 20, 22, 38].

The main difficulty of neural ODE is the memory footprint [1, 9, 39]. For an accurate integration, one has to make a step size smaller and to employ a higher-order numerical integrator composed of many internal stages. A neural network is used at each stage of each time step, and the backpropagation algorithm requires a memory footprint linearly proportional to the number of uses times the network size [32]. To reduce the memory footprint, the adjoint method has been employed, which obtains the

gradient by a backward integration of an adjoint variable together with the state  $x$  [1, 7, 16, 34, 37]. However, the adjoint method requires a sufficiently small time step, or it suffers from numerical errors. We summarize two issues of the adjoint method with a numerical integrator; (a) the backward integration of the state  $x$  is not consistent with the forward integration, and (b) the backward integration of the adjoint variable is not consistent with the gradient. Several existing methods employed the checkpointing scheme to solve the issue (a), and applied the backpropagation algorithm to a subset of the integration to solve the issue (b) [9, 39, 40]. These methods still require a large memory footprint for the backpropagation algorithm over time steps and internal stages.

To overcome these issues with a minimal memory footprint, this study proposes *symplectic adjoint method*. The main contribution of the symplectic adjoint method is three-folds.

**Exact Gradient:** The adjoint method relies on a quadratic invariant of a partitioned system, but a numerical integrator cannot preserve such quantity in general. The proposed symplectic adjoint method employs a specially-designed integrator, which preserves a quadratic invariant in discrete time, and thereby provides the exact gradient.

**Minimal Memory Footprint:** Existing methods that obtain the exact gradient (i.e., solve the issue (b)) employed the backpropagation algorithm to obtain the gradient over steps and stages [9, 39, 40]; the memory footprint is proportional to the number of steps/stages *times* the network size. Conversely, the proposed symplectic adjoint method only applies the backpropagation algorithm to each use of the neural network by a specially-designed integrator, and the memory footprint is proportional to the number of steps/stages *plus* the network size.

**Robust to Rounding Error:** When applying the backpropagation algorithm to an integration over many time steps, the algorithm accumulates the gradient from each use of the neural network, and suffers from the rounding error [39]. The proposed symplectic adjoint method obtains the gradient from each step as a numerical integration, and hence, it is more robust to the rounding error.

## 2 Background and Related Work

### 2.1 Neural Ordinary Differential Equation and Adjoint Method

We use the following notions;

- $M$ : the number of stacked neural ODE components,
- $L$ : the number of layers in a neural network,
- $N$ : the number of discretized time steps between  $t = 0$  and  $t = T$ , and
- $s$ : the number of uses of a neural network  $f$  per step.

$s$  is typically equal to the number of stages of the numerical integrator [16]. A numerical integration forward in time requires computational cost of  $O(MNsL)$ . The numerical integration also provides a computational graph over time steps, which is retained with a memory footprint of  $O(MNsL)$ , and then the backpropagation algorithm is applied to obtain the gradient. The total computational cost is of  $O(2MNsL)$ , where we suppose the computational cost of the backpropagation algorithm is equal to that of the forward propagation. We summarize the memory footprint and computational cost in Table 1.

To reduce the memory footprint, the original study on neural ODE introduced the adjoint method [1, 7, 16, 34, 37]. The adjoint method integrates a pair of the system state  $x$  and the adjoint variable  $\lambda$  backward in time. The adjoint variable  $\lambda$  represents the gradient  $\frac{\partial \mathcal{L}}{\partial x}$  of some function  $\mathcal{L}$ , and the adjoint method works as backpropagation (or more generally the reverse-mode automatic differentiation) in continuous-time. The memory footprint is of  $O(M)$  to retain the final conditions  $x(T)$  of  $M$  neural ODE components and of  $O(L)$  to obtain the gradient of a neural network  $f$  for the adjoint variable  $\lambda$ . The computational cost to obtain the gradient is doubled due to the re-integration of the system state  $x$  backward in time.

The adjoint method only holds in continuous time, but it does not provide the exact gradient with a numerical integrator [9, 34]. A small step size reduces the numerical error, but leads to a longer computation time and a rounding error. Conversely, the proposed symplectic adjoint method uses a specially-designed integrator, which provides the exact gradient in discrete time and thereby solves the issue (b).

Table 1: Comparison with Other Studies

Methods	Gradient Calculation	Exact	Checkpoint	Memory Footprint	Computational Cost
NODE [1]	adjoint method	no	$x_N$	$O(M) + O(L)$	$O(3MN_sL)$
NODE [1]	backpropagation	yes	—	$O(MN_sL)$	$O(2MN_sL)$
ANODE [9]	backpropagation	yes	$x_0$	$O(M) + O(NsL)$	$O(3MN_sL)$
ACA [39]	backpropagation	yes	$\{x_n\}_{n=0}^{N-1}$	$O(MN) + O(sL)$	$O(3MN_sL)$
MALI [40]*	backpropagation	yes	$x_N$	$O(M) + O(sL)$	$O(4MN_sL)$
proposed**	symplectic adjoint method	yes	$\{x_n\}_{n=0}^{N-1}, \{X_{n,i}\}_{i=1}^s$	$O(MN+s) + O(L)$	$O(4MN_sL)$

\* Available only for the leap-frog integrator. \*\* Available for any Runge-Kutta methods.

## 2.2 Checkpointing Scheme

In general, the checkpointing scheme has been investigated to reduce the memory footprint of neural networks [13, 14], where intermediate states are retained sparsely as checkpoints, and a computational graph is recomputed from each checkpoint. For example, Gruslys *et al.* applied it to recurrent neural networks [14]. The checkpointing scheme uses a checkpoint as a solution to the issue (a) and the backpropagation algorithm as a solution to the issue (b). ANODE is a scheme that retains the initial value  $x(0)$  of each neural ODE component, and solves the initial value problem again for the backpropagation algorithm [9]. The memory footprint is of  $O(M)$  to retain the initial conditions of  $M$  components and of  $O(NsL)$  to obtain the gradient of each component; ANODE does not reduce the memory footprint when  $M = 1$ . ACA is a scheme that retains all steps  $\{x_n\}_{n=0}^{N-1}$  as checkpoints with a memory footprint of  $O(MN)$  [39]. From each checkpoint  $x_n$ , the scheme recalculates the next step  $x_{n+1}$ , and obtains the gradient by the backpropagation algorithm with a memory footprint of  $O(sL)$ . Even with checkpoints, the memory footprint is still proportional to the number  $s$  of uses of a neural network  $f$  per step, which is not negligible for a high-order integrator, e.g.,  $s = 6$  for the Dormand-Prince method. In this context, the proposed method is regarded as a checkpointing scheme inside of a numerical integrator, and hence it solves the issue (a).

Instead of a checkpointing scheme, MALI employed the leapfrog integrator, which is time-reversible and hence enables the backward integration consistent with the forward integration (i.e., solves the issue (a)) [40]. However, this approach is obviously available only for time-reversible integrators, while explicit Runge-Kutta methods are not. A similar approach was proposed as RevNet, which is a special residual architecture [10]. When considering ResNet as the forward Euler method [1, 17], RevNet can be considered as the leapfrog integrator and can recalculate the intermediate states from the output to the input [16].

## 3 Adjoint Method

Consider a differential system

$$\frac{d}{dt}x = f(x, t, \theta), \quad (1)$$

where  $x$  denotes the system state,  $t$  denotes the independent variable (e.g., the time), and  $\theta$  denotes the parameters of the function  $f$ . Given an initial condition  $x(0) = x_0$ , the solution  $x(t)$  is given by

$$x(t) = x_0 + \int_0^t f(x(\tau), \tau, \theta) d\tau. \quad (2)$$

The solution is evaluated at the terminal  $t = T$  by a function  $\mathcal{L}$  as  $\mathcal{L}(x(T))$ . The main interest is in obtaining the gradients of the function  $\mathcal{L}$  with respect to the initial condition  $x_0$  and the parameters  $\theta$ . For simplicity, we focus on the initial condition  $x_0$  and omit the parameters  $\theta$ .

We introduce the adjoint method [1, 7, 16, 34, 37], which is based on the *variational variable*  $\delta(t)$  and the *adjoint variable*  $\lambda(t)$ . These variables follow the variational system and adjoint system as

$$\frac{d}{dt}\delta(t) = \frac{\partial f}{\partial x}(x(t), t)\delta(t) \text{ for } \delta(0) = I, \quad \frac{d}{dt}\lambda(t) = -\frac{\partial f}{\partial x}(x(t), t)^\top\lambda(t) \text{ for } \lambda(T) = \lambda_T. \quad (3)$$

The variational variable  $\delta(t)$  represents the Jacobian  $\frac{\partial x(t)}{\partial x_0}$  of the state  $x(t)$  w.r.t. the initial condition  $x_0$ ; the detailed derivation is summarized in Appendix A.

**Remark 1.** The quantity  $\lambda^\top \delta$  is time-invariant, i.e.,  $\lambda(t)^\top \delta(t) = \lambda(0)^\top \delta(0)$ .

The proofs of most Remarks and Theorems in this paper are summarized in Appendix B.

**Remark 2.**  $\lambda(t)$  represents the gradient  $(\frac{\partial \mathcal{L}(x(T))}{\partial x(t)})^\top$  if the final condition  $\lambda_T$  of the adjoint variable  $\lambda$  is set to  $(\frac{\partial \mathcal{L}(x(T))}{\partial x(T)})^\top$ .

**Proof of Remark 2:** Since  $\delta(t) = \frac{\partial x(t)}{\partial x_0}$  and  $\lambda^\top \delta$  is time-invariant,

$$\frac{\partial \mathcal{L}(x(T))}{\partial x_0} = \frac{\partial \mathcal{L}(x(T))}{\partial x(T)} \frac{\partial x(T)}{\partial x_0} = \lambda(T)^\top \delta(T) = \lambda(t)^\top \delta(t) = \frac{\partial \mathcal{L}(x(t))}{\partial x(t)} \frac{\partial x(t)}{\partial x_0}. \quad (4)$$

Hence, the backward integration of the adjoint variable  $\lambda(t)$  works as the reverse-mode automatic differentiation. See Appendix C for more general cases; the gradient w.r.t. parameters  $\theta$  and the gradient of a functional  $\mathcal{C}$ .

According to the original implementation of neural ODE [1], the final condition  $x(T)$  of the system state  $x$  is retained after the forward integration, and the pair of the system state  $x$  and the adjoint variable  $\lambda$  is integrated backward in time to take the gradients. The right-hand sides of the main system in Eq. (1) and the adjoint system in Eq. (3) are obtained by the forward and backward propagations of the function  $f$ , respectively. Hence, the computational cost of the adjoint method is twice as much as that of the ordinary backpropagation algorithm.

However, after a numerical integrator discretizes the time, Remark 1 does not hold, and hence the adjoint variable  $\lambda(t)$  is not equal to the exact gradient [9, 34] (the issue (b)). Moreover, the numerical integration backward in time is not consistent with that forward in time (the issue (a)). A small step size (i.e., a small tolerance) surpasses the numerical error, but at the same time, it leads to a longer computation time and a rounding error. This fact motivates the present study to obtain the exact gradient with a small memory footprint.

## 4 Symplectic Adjoint Method

### 4.1 Runge-Kutta Method

We first discretize the main system in Eq. (1). Let  $t_n$ ,  $h_n$ , and  $x_n$  denote the  $n$ -th time step, step size, and state, respectively, where  $h_n = t_{n+1} - t_n$ . For solving the system state  $x(t)$ , most previous studies employed one of Runge-Kutta methods, which is generally expressed as

$$\begin{aligned} x_{n+1} &= x_n + h_n \sum_{i=1}^s b_i k_{n,i}, \\ k_{n,i} &:= f(X_{n,i}, t_n + c_i h_n), \\ X_{n,i} &:= x_n + h_n \sum_{j=1}^s a_{i,j} k_{n,j}. \end{aligned} \quad (5)$$

The coefficients  $a_{i,j}$ ,  $b_i$ , and  $c_i$  are often summarized as Butcher tableau [15, 16, 34]. If  $a_{i,j} = 0$  for  $j \geq i$ , the intermediate state  $X_{n,i}$  is calculable from  $i = 1$  to  $i = s$  sequentially; then, the Runge-Kutta method is considered explicit.

**Remark 3.** When the system in Eq. (1) is solved by the Runge-Kutta method in Eq. (5), the variational system in Eq. (3) is automatically solved by the same Runge-Kutta method.

Hence, the variational variable  $\delta(t)$  is not necessarily solved separately. The Runge-Kutta methods are not time-reversible, i.e., the numerical integration backward in time is not consistent with that forward in time.

### 4.2 Symplectic Runge-Kutta Method

We assume  $b_i \neq 0$  for  $i = 1, \dots, s$ . We suppose the adjoint system to be solved by another Runge-Kutta method expressed as

$$\begin{aligned} \lambda_{n+1} &= \lambda_n + h_n \sum_{i=1}^s B_i l_{n,i}, \\ l_{n,i} &:= -\frac{\partial f}{\partial x}(X_{n,i}, t_n + C_i h_n)^\top \Lambda_{n,i}, \\ \Lambda_{n,i} &:= \lambda_n + h_n \sum_{j=1}^s A_{i,j} l_{n,j}. \end{aligned} \quad (6)$$

The final condition  $\lambda_N$  is set to  $\frac{\partial \mathcal{L}(x_N)}{\partial x_N}$ . Since the time evolutions of the variational variable  $\delta$  and the adjoint variable  $\lambda$  are expressible by two equations, the combined system is considered as a partitioned system. A combination of two Runge-Kutta methods for solving a partitioned system is called a partitioned Runge-Kutta method, where  $C_i = c_i$  for  $i = 1, \dots, s$ . We introduce the following condition for a partitioned Runge-Kutta method.

**Condition 1.**  $b_i A_{i,j} + B_j a_{j,i} - b_i B_j = 0$  for  $i, j = 1, \dots, s$ , and  $B_i = b_i \neq 0$  and  $C_i = c_i$  for  $i = 1, \dots, s$ .

**Theorem 1.** A partitioned Runge-Kutta method in Eqs. (5) and (6) conserves a bilinear quantity  $S(\delta, \lambda)$  if the continuous-time system conserves the quantity  $S(\delta, \lambda)$  and Condition 1 holds.

One of the most popular Runge-Kutta methods, the Dormand-Prince method, has  $b_2 = 0$  [6]. For such methods, we generalize the Runge-Kutta method under Condition 1 in Eq. (6) as

$$\begin{aligned} \lambda_{n+1} &= \lambda_n + h_n \sum_{i=1}^s \tilde{b}_i l_{n,i}, \\ l_{n,i} &:= -\frac{\partial f}{\partial x}(X_{n,i}, t_n + c_i h_n)^\top \Lambda_{n,i}, \\ \Lambda_{n,i} &:= \begin{cases} \lambda_n + h_n \sum_{j=1}^s \tilde{b}_j \left(1 - \frac{a_{j,i}}{b_i}\right) l_{n,j} & \text{if } i \notin I_0 \\ -\sum_{j=1}^s \tilde{b}_j a_{j,i} l_{n,j} & \text{if } i \in I_0, \end{cases} \end{aligned} \quad (7)$$

where

$$\tilde{b}_i = \begin{cases} b_i & \text{if } i \notin I_0 \\ h_n & \text{if } i \in I_0, \end{cases}, \quad I_0 = \{i | i = 1, \dots, s, b_i = 0\}. \quad (8)$$

Note that this numerical integrator is no longer a Runge-Kutta method.

**Theorem 2.** The combination of the integrators in Eqs. (5) and (7) conserves a bilinear quantity  $S(\delta, \lambda)$  if the continuous-time system conserves the quantity  $S(\delta, \lambda)$ . Then, the adjoint variable  $\lambda$  represents the gradient  $\lambda_n = (\frac{\partial \mathcal{L}(x_n)}{\partial x_n})^\top$ .

**Remark 4.** The Runge-Kutta method in Eq. (6) under Condition 1 and the numerical integrator in Eq. (7) are explicit backward in time if the Runge-Kutta method in Eq. (5) is explicit.

### 4.3 Implementation of Symplectic Adjoint Method

The discrete-time adjoint system in Eq. (7) depends on the intermediate system state  $X_{n,i}$  and the vector-Jacobian product (VJP)  $\lambda^\top \frac{\partial f}{\partial x}$ . To obtain the VJP  $\lambda^\top \frac{\partial f}{\partial x}$ , the computational graph from the input  $X_{n,i}$  to the output  $f(X_{n,i}, t_n + c_i h_n)$  is required. When all computational graphs are retained in the forward integration, the memory footprint and the computational cost are of the same orders as those for the naive backpropagation algorithm. To surpass the memory footprint, we propose the following strategy as summarized in Algorithms 1 and 2.

At the forward integration of a neural ODE component, pairs of system states  $x_n$  and time steps  $t_n$  are retained with a memory of  $O(N)$  as checkpoints, and any computational graphs are discarded, as shown in Algorithm 1. The backward integration is summarized in Algorithm 2. The system state  $x$  is integrated from a checkpoint  $x_n$  to the next step  $x_{n+1}$  following the Runge-Kutta method in Eq. (5) with all intermediate states  $X_{n,i}$  retained as checkpoints with a memory of  $O(s)$  and all computational graphs discarded. Then, the adjoint system is integrated from  $n+1$  to  $n$  using Eq. (7). Since the computational graph of the neural network  $f$  in line 5 is discarded, obtaining the VJP  $\lambda^\top \frac{\partial f}{\partial x}$  in line 11 needs a computational cost of  $O(2L)$  and a memory of  $O(L)$ . The above steps are repeated from  $n = N-1$  to  $n = 0$ . Hence, the total memory footprint is  $O(MN + s) + O(L)$  for  $M$  neural ODE components at most. We emphasize that the memory footprint is proportional to the number of checkpoints  $MN + s$  plus the neural network size  $L$ , while existing methods need the memory footprint proportional to the number of checkpoints plus the number of integration steps/stages between two checkpoints (that is,  $Ns$  for ANODE and  $s$  for ACA) times the neural network size  $L$  (see Table 1). Due to the recalculation of a discarded computational graph of  $f$  in line 11, the computational cost of the proposed strategy is of  $O(4MNsL)$  while those of the adjoint method [1] and ACA [39] are of  $O(3MNsL)$ . However, as demonstrated later, the increased in the computation time is much less than theory due to other bottlenecks.

The proposed strategy obtains the system state  $x_n$  consistent with that in the forward integration thanks to the checkpoints (i.e., solves the issue (a)), and obtains the exact gradient as the adjoint variable  $\lambda$  thanks to the symplectic Runge-Kutta method (i.e., solves the issue (b)).

---

**Algorithm 1** Forward Integration

---

**Input:**  $x_0$   
**Output:**  $x_N, \{x_n\}_{n=0}^{N-1}$

- 1: **for**  $n = 0$  to  $N - 1$  **do**
- 2:   Retain  $x_n$  as a checkpoint.  
      According to Eq. (5)
- 3:   **for**  $i = 1$  to  $s$  **do**
- 4:     Get  $X_{n,i}$  using  $x_n$  and  $k_{n,j}$  for  $j < i$ .
- 5:     Get  $k_{n,i}$  using  $X_{n,i}$ .
- 6:   **end for**
- 7:     Get  $x_{n+1}$  using  $x_n$  and  $k_{n,j}$ .
- 8: **end for**

---

A partitioned Runge-Kutta method that satisfies Condition 1 is symplectic and conserves the symplectic structure of Hamiltonian system [15, 16]. While the symplecticity is sufficient but not necessary for obtaining the exact gradient, we named the above strategy as *symplectic adjoint method*.

---

**Algorithm 2** Backward Integration

---

**Input:**  $x_N, \{x_n\}_{n=0}^{N-1}$   
**Output:**  $\lambda_0$

- 1: **for**  $n = N - 1$  to  $0$  **do**
- 2:   Load checkpoint  $x_n$ .  
      According to Eq. (5)
- 3:   **for**  $i = 1$  to  $s$  **do**
- 4:     Get  $X_{n,i}$  using  $x_n$  and  $k_{n,j}$  for  $j < i$ .
- 5:     Get  $k_{n,i}$  using  $X_{n,i}$ .
- 6:     Retain  $X_{n,i}$  as a checkpoint.
- 7: **end for**
- 8:   According to Eq. (7)
- 9:   **for**  $i = s$  to  $1$  **do**
- 10:     Get  $\Lambda_{n,i}$  using  $\lambda_{n+1}$  and  $l_{n,j}$  for  $j > i$ .
- 11:     Load checkpoint  $X_{n,i}$ .
- 12:     Get  $l_{n,i}$  using  $\Lambda_{n,i}$  and  $X_{n,i}$ .
- 13:     Discard checkpoint  $X_{n,i}$ .
- 14: **end for**
- 15:     Get  $\lambda_n$  using  $\lambda_{n+1}$  and  $l_{n,i}$ .
- 16:     Discard checkpoint  $x_n$ .
- 16: **end for**

---

## 5 Experiments

We evaluated the performances of the proposed symplectic adjoint method and competitive methods using PyTorch 1.7.1 [29]. We implemented the proposed symplectic adjoint method by extending the adjoint method implemented in the package `torchdiffeq` 0.1.1 [1]. We also reimplemented ANODE [9] and ACA [39] since their official implementations have interfaces incompatible with `torchdiffeq`. The source code is available at [https://github.com/\\*\\*\\*\\*\\*/symplectic-adjoint-method/](https://github.com/*****/symplectic-adjoint-method/).

### 5.1 Continuous Normalizing Flow

**Experimental Settings:** We evaluated the proposed symplectic adjoint method on training continuous normalizing flows [1, 11]. A normalizing flow is a neural network that approximates a bijective map  $g$  and obtains the exact likelihood of a sample  $u$  by the change of variables  $\log p(u) = \log p(z) + \log |\det \frac{\partial g(u)}{\partial u}|$ , where  $z = g(u)$  and  $p(z)$  denote the corresponding latent variable and its prior, respectively [4, 5, 31]. A continuous normalizing flow is a normalizing flow whose map  $g$  is modeled by stacked neural ODE components, in particular,  $u = x(0)$  and  $z = x(T)$  for the case with  $M = 1$  [1, 11]. The log-determinant of the Jacobian is obtained by a numerical integration together with the system state  $x$  as  $\log |\det \frac{\partial g(u)}{\partial u}| = - \int_0^T \text{Tr}(\frac{\partial f}{\partial x}(x(t), t) dt$ . The trace operation  $\text{Tr}$  is approximated by Hutchinson's estimator [19]. We followed the experimental settings of a continuous normalizing flow, FFJORD [11], unless otherwise stated.

We obtained five real tabular datasets, namely MINIBOONE, GAS, POWER, HEPMASS, and BSDS300 datasets [11, 27]. The network architectures were the same as those that achieved the best results in the original experiments; the number  $M$  of neural ODE components varied across datasets. We employed the Dormand-Prince integrator, which is a fourth-order Runge-Kutta method with an adaptive time stepping, composed of seven stages [6]. Note that the number of function evaluations is  $s = 6$  because the last stage is reused as the first stage of the next step. We set the absolute and relative tolerances to  $\text{atol} = 10^{-8}$  and  $\text{rtol} = 10^{-6}$ , respectively. The neural networks were trained using Adam optimizer [23] with a learning rate of  $10^{-3}$ . We used a batch-size of 1,000 for all datasets to put a mini-batch into a single NVIDIA GeForce 2080Ti GPU with a memory of 11 GiB, while the original experiments employed a batch-size of 10,000 for the latter three datasets on multiple GPUs. When using multiple GPUs, bottlenecks such as transferring data across GPUs may affect on the performances, and a fair comparison becomes difficult. Nonetheless, the naive backpropagation algorithm and ANODE ran out the memory for BSDS300 dataset.

Table 2: The results on continuous normalizing flows.

	MINIBOONE ( $M = 1$ )			GAS ( $M = 5$ )			POWER ( $M = 5$ )		
	NLL	mem.	time	NLL	mem.	time	NLL	mem.	time
adjoint method [1]	10.59 $\pm$ 0.17	156	0.90	-10.53 $\pm$ 0.25	19	5.71	-0.31 $\pm$ 0.01	<b>6.8</b>	7.67
backpropagation [1]	10.54 $\pm$ 0.18	4505	1.13	-9.53 $\pm$ 0.42	4,540	16.31	-0.24 $\pm$ 0.05	1,666.4	14.17
ANODE [9]	10.54 $\pm$ 0.18	4527	1.27	-9.53 $\pm$ 0.42	1,892	6.11	-0.24 $\pm$ 0.05	542.6	5.40
ACA [39]	10.57 $\pm$ 0.30	292	0.91	-10.65 $\pm$ 0.45	66	4.72	-0.31 $\pm$ 0.02	25.4	5.78
proposed	10.49 $\pm$ 0.11	<b>82</b>	1.05	-10.89 $\pm$ 0.11	<b>15</b>	5.60	-0.31 $\pm$ 0.02	8.0	7.09

	HEPMASS ( $M = 10$ )			BSDS300 ( $M = 2$ )			MNIST ( $M = 6$ )		
	NLL	mem.	time	NLL	mem.	time	NLL	mem.	time
adjoint method [1]	16.49 $\pm$ 0.25	27	4.99	-152.04 $\pm$ 0.09	473	12.08	0.95	<b>1,052</b>	16.28
backpropagation [1]	17.03 $\pm$ 0.22	5155	14.47	—	—	—	—	—	—
ANODE [9]	17.03 $\pm$ 0.22	1154	4.85	—	—	—	0.95	36,391	12.19
ACA [39]	16.41 $\pm$ 0.39	72	4.37	-151.27 $\pm$ 0.47	656	7.82	0.95	4,310	10.32
proposed	16.48 $\pm$ 0.20	<b>22</b>	4.94	-151.17 $\pm$ 0.15	<b>184</b>	8.12	0.95	1,058	12.17

Negative log-likelihoods (NLL), memory footprint [MiB], and computation time per iteration [s/itr].

We also obtained MNIST dataset [24]. For this dataset, we used a single NVIDIA GeForce RTX 8000 GPU with a memory of 48 GiB. We employed the multi-scale architecture, and set a batch-size to 200 and the tolerance to  $\text{atol} = \text{rtol} = 10^{-5}$ . We truncated the training procedure at the 250th epoch because the performances almost converged to a level better than the original study. The naive backpropagation algorithm ran out the memory.

**Performances:** The medians  $\pm$  standard derivations of 3 runs are summarized in Table 2. All methods obtained models of negative log-likelihoods (NLLs) at a similar level because all but the adjoint method provide the exact gradients up to rounding error, and the adjoint method with a small tolerance provides a sufficiently accurate gradient. The naive backpropagation algorithm and ANODE obtained slightly worse results on GAS, POWER, and HEPMASS datasets. Due to the adaptive time stepping, the numerical integrator sometimes makes a step size much smaller, and the backpropagation algorithm over time steps suffered from rounding errors, as pointed out by Zhuang *et al.* [39]. Conversely, the ACA and proposed symplectic adjoint method applied the backpropagation algorithm separately to a subset of the integration (i.e., each step composed of  $s$  stages for the ACA, and each stage for the (symplectic) adjoint method), and thereby, become robust to rounding errors (See Appendix D for details).

After the training procedure, we obtained the maximum memory footprint during additional training iterations (see mem. [MiB]), from which we subtracted the memory footprint without training (i.e., occupied by the model parameters, optimizer, loaded data, and so on). The results roughly agree with the theoretical orders shown in Table 1. The proposed symplectic adjoint method occupied a memory footprint compatible to or smaller than the adjoint method and much smaller than the other methods. The adjoint method needed an additional memory for the adaptive time stepping in the backward integration.

On the other hand, the computation time per iteration (time [s/itr]) at the end of the training procedure does not agree with the theoretical orders. Firstly, the naive backpropagation algorithm and ANODE were slower than expected in many cases. A method with a large memory footprint may have to wait for memory to be freed, leading to an additional bottleneck. Secondly, the adjoint method was slower than expected in many cases, especially for BSDS300 and MNIST datasets. For obtaining the gradients, the adjoint method integrates the adjoint variable  $\lambda$ , which has the size same as the parameters  $\theta$  and much larger than the system state  $s$ ; an accurate backward integration needs a much smaller step size than the forward integration, leading to a longer computation time. The proposed symplectic adjoint method is free from the above bottlenecks and functions faster in practice; it was faster than the adjoint method for all but MINIBOONE dataset.

Table 3: The results on learning physical systems.

	KdV Equation			Cahn-Hilliard System		
	MSE ( $\times 10^{-3}$ )	mem.	time	MSE ( $\times 10^{-6}$ )	mem.	time
adjoint method [1]	1.87 $\pm$ 3.08	46	0.286	5.93 $\pm$ 2.97	46	0.93
backpropagation [1]	1.87 $\pm$ 3.08	647	0.084	5.66 $\pm$ 1.15	3,045	0.37
ACA [39]	1.87 $\pm$ 3.08	601	0.108	4.93 $\pm$ 1.14	600	0.45
proposed	1.87 $\pm$ 3.08	<b>33</b>	0.158	5.60 $\pm$ 1.32	<b>33</b>	0.53

Mean-squared errors (MSEs) in long-term predictions, memory footprint [MiB], and computation time per iteration [s/itr].

**Robustness to Tolerance:** The adjoint method provides an approximated gradient only with a small tolerance. To evaluate the robustness against the tolerance, we employed MINIBOONE dataset and varied the absolute tolerance  $atol$  while keeping the relative one as  $rtol = 10^2 \times atol$ . After training, we obtained the NLLs and computation times with  $atol = 10^{-8}$  as summarized in Fig. 1. The adjoint method worked well only with  $atol < 10^{-4}$ ; otherwise, the numerical error in the backward integration was non-negligible, and the performance was degraded. The proposed symplectic adjoint method worked well even with  $atol = 10^{-4}$  because it provides the exact gradient regardless of the tolerances. With  $atol > 10^{-4}$ , the numerical error in the forward integration was non-negligible, and the adjoint method was destabilized. Even then, the proposed symplectic adjoint method worked at a certain level. The proposed symplectic adjoint method is robust to a large tolerance and potentially works faster with an appropriate tolerance.

## 5.2 Continuous-Time Dynamical System

**Experimental Settings:** We evaluated the proposed symplectic adjoint method on learning continuous-time dynamical systems [12, 26, 33]. Many physical phenomena can be modeled using the gradient of system energy  $H$  as  $dx/dt = G\nabla H(x)$ , where  $G$  is a coefficient matrix that determines the behaviors of the energy and, for a partially differential equation (PDE) system, the mass [8]. We followed the experimental settings of HNN++ [26]. A three-layered neural network approximated the energy function  $H$  and learned time series by interpolating two successive samples. We employed two physical systems described by PDEs, namely the Korteweg-de Vries (KdV) equation and the Cahn-Hilliard system. We used a batch-size of 100 to put a mini-batch into a single NVIDIA TITAN V GPU instead of the original batch-size of 200. Moreover, we used the eighth-order Dormand-Prince method, composed of 13 stages, to emphasize the efficiency of the proposed method [16]. We omitted ANODE because of  $M = 1$ . We evaluated the performances using mean-squared errors (MSEs) in the system energy for long-term predictions.

**Performances:** The medians of 3 runs are summarized in Table 3. Due to the accumulated error in the numerical integration, the MSEs have large variances, but all methods obtained MSEs at a similar level. Because of the large number of stages, the ACA needed a much larger memory footprint than the proposed symplectic adjoint method; the proposed symplectic adjoint method is more beneficial for physical simulations, which often require extremely higher-order integrators. The computation times nearly agree with the theoretical orders except for the adjoint method.

## 6 Conclusion

We proposed the symplectic adjoint method. The backward integration is consistent with the forward integration thanks to a checkpointing scheme, and the adjoint variable represents the exact gradient thanks to a symplectic Runge-Kutta method. Thereby, the symplectic adjoint method obtains the exact gradient of a differential system with a minimal memory footprint among competitive methods,

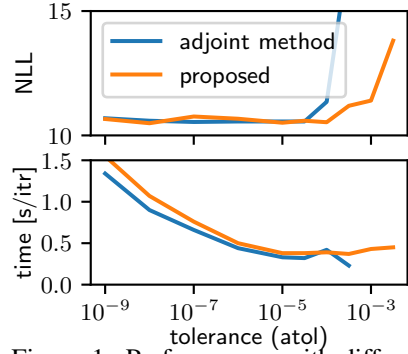


Figure 1: Performances with different tolerances.

as demonstrated by the experiments. Despite the theoretical value, the symplectic adjoint method works faster than the adjoint method in many cases.

This study was partially supported by CREST Grant Number JPMJCR1914.

## References

- [1] Chen, T. Q., Rubanova, Y., Bettencourt, J., Duvenaud, D., Chen, R. T. Q., Rubanova, Y., Bettencourt, J., and Duvenaud, D. (2018). Neural Ordinary Differential Equations. In *Advances in Neural Information Processing Systems (NeurIPS)*, pages 1–19.
- [2] Chen, Z., Zhang, J., Arjovsky, M., and Bottou, L. (2020). Symplectic Recurrent Neural Networks. In *International Conference on Learning Representations (ICLR)*, pages 1–23.
- [3] Devlin, J., Chang, M.-W., Lee, K., and Toutanova, K. (2018). BERT: Pre-training of Deep Bidirectional Transformers for Language Understanding. *arXiv*, pages 1–15.
- [4] Dinh, L., Krueger, D., and Bengio, Y. (2014). NICE: Non-linear Independent Components Estimation. In *Workshop on International Conference on Learning Representations*, volume 1, pages 1–13.
- [5] Dinh, L., Sohl-Dickstein, J., and Bengio, S. (2017). Density estimation using Real NVP. In *International Conference on Learning Representations (ICLR)*, pages 1–32.
- [6] Dormand, J. R. and Prince, P. J. (1986). A reconsideration of some embedded Runge-Kutta formulae. *Journal of Computational and Applied Mathematics*, 15(2):203–211.
- [7] Errico, R. M. (1997). What Is an Adjoint Model? *Bulletin of the American Meteorological Society*, 78(11):2577–2591.
- [8] Furihata, D. and Matsuo, T. (2010). *Discrete Variational Derivative Method: A Structure-Preserving Numerical Method for Partial Differential Equations*. Chapman and Hall/CRC.
- [9] Gholami, A., Keutzer, K., and Biros, G. (2019). ANODE: Unconditionally accurate memory-efficient gradients for neural ODEs.
- [10] Gomez, A. N., Ren, M., Urtasun, R., and Grosse, R. B. (2017). The Reversible Residual Network: Backpropagation Without Storing Activations. pages 1–14.
- [11] Grathwohl, W., Chen, R. T. Q., Bettencourt, J., Sutskever, I., and Duvenaud, D. (2018). FFJORD: Free-form Continuous Dynamics for Scalable Reversible Generative Models. pages 1–13.
- [12] Greydanus, S., Dzamba, M., and Yosinski, J. (2019). Hamiltonian Neural Networks. In *Advances in Neural Information Processing Systems (NeurIPS)*, pages 1–16.
- [13] Griewank, A. and Walther, A. (2000). Algorithm 799: Revolve: An implementation of checkpointing for the reverse or adjoint mode of computational differentiation. *ACM Transactions on Mathematical Software*, 26(1):19–45.
- [14] Gruslys, A., Munos, R., Danihelka, I., Lanctot, M., and Graves, A. (2016). Memory-efficient backpropagation through time. *Advances in Neural Information Processing Systems (NIPS)*, pages 4132–4140.
- [15] Hairer, E., Lubich, C., and Wanner, G. (2006). *Geometric Numerical Integration: Structure-Preserving Algorithms for Ordinary Differential Equations*, volume 31 of *Springer Series in Computational Mathematics*. Springer-Verlag, Berlin/Heidelberg.
- [16] Hairer, E., Nørsett, S. P., and Wanner, G. (1993). *Solving Ordinary Differential Equations I: Nonstiff Problems*, volume 8 of *Springer Series in Computational Mathematics*. Springer Berlin Heidelberg, Berlin, Heidelberg.
- [17] He, K., Zhang, X., Ren, S., and Sun, J. (2016). Deep Residual Learning for Image Recognition. In *IEEE Conference on Computer Vision and Pattern Recognition (CVPR)*, pages 1–9.
- [18] Hochreiter, S. and Schmidhuber, J. (1997). Long Short-Term Memory. *Neural Computation*, 9(8):1735–1780.
- [19] Hutchinson, M. (1990). A stochastic estimator of the trace of the influence matrix for laplacian smoothing splines. *Communications in Statistics - Simulation and Computation*, 19(2):433–450.

[20] Jiang, C. M., Huang, J., Tagliasacchi, A., and Guibas, L. (2020). ShapeFlow: Learnable Deformations Among 3D Shapes. In *Advances in Neural Information Processing Systems (NeurIPS)*.

[21] Kidger, P., Morrill, J., Foster, J., and Lyons, T. (2020). Neural Controlled Differential Equations for Irregular Time Series. In *Advances in Neural Information Processing Systems (NeurIPS)*, number 1.

[22] Kim, H., Lee, H., Kang, W. H., Cheon, S. J., Choi, B. J., and Kim, N. S. (2020). WaveNODE: A Continuous Normalizing Flow for Speech Synthesis. In *ICML2020 Workshop on Invertible Neural Networks, Normalizing Flows, and Explicit Likelihood Models*, number Icml.

[23] Kingma, D. P. and Ba, J. (2015). Adam: A Method for Stochastic Optimization. In *International Conference on Learning Representations (ICLR)*, pages 1–15.

[24] LeCun, Y., Bottou, L., Bengio, Y., and Haffner, P. (1998). Gradient-based learning applied to document recognition. In *Proceedings of the IEEE*, volume 86, pages 2278–2323.

[25] Lu, Y., Zhong, A., Li, Q., and Dong, B. (2018). Beyond finite layer neural networks: Bridging deep architectures and numerical differential equations. *35th International Conference on Machine Learning, ICML 2018*, 7:5181–5190.

[26] Matsubara, T., Ishikawa, A., and Yaguchi, T. (2020). Deep Energy-Based Modeling of Discrete-Time Physics. In *Advances in Neural Information Processing Systems (NeurIPS)*.

[27] Papamakarios, G., Pavlakou, T., and Murray, I. (2017). Masked Autoregressive Flow for Density Estimation. In *Advances in Neural Information Processing Systems (NIPS)*, pages 1–17.

[28] Pascanu, R., Mikolov, T., and Bengio, Y. (2013). On the difficulty of training Recurrent Neural Networks. In *International Conference on Machine Learning (ICML)*, pages 2347–2355.

[29] Paszke, A., Chanan, G., Lin, Z., Gross, S., Yang, E., Antiga, L., and Devito, Z. (2017). Automatic differentiation in PyTorch. In *Autodiff Workshop on Advances in Neural Information Processing Systems*, pages 1–4.

[30] Rana, M. A., Li, A., Fox, D., Boots, B., Ramos, F., and Ratliff, N. (2020). Euclideanizing Flows: Diffeomorphic Reduction for Learning Stable Dynamical Systems. 120:1–10.

[31] Rezende, D. J. and Mohamed, S. (2015). Variational Inference with Normalizing Flows. In *International Conference on Machine Learning (ICML)*, volume 37, pages 3–6.

[32] Rumelhart, D. E., Hinton, G. E., and Williams, R. J. (1986). Learning representations by back-propagating errors. *Nature*, 323(6088):533–536.

[33] Saemundsson, S., Terenin, A., Hofmann, K., Deisenroth, M. P., Sæmundsson, S., Hofmann, K., Terenin, A., and Deisenroth, M. P. (2020). Variational Integrator Networks for Physically Meaningful Embeddings. In *Artificial Intelligence and Statistics (AISTATS)*, volume 108, pages 1–11.

[34] Sanz-Serna, J. M. (2016). Symplectic Runge-Kutta schemes for adjoint equations, automatic differentiation, optimal control, and more. *SIAM Review*, 58(1):3–33.

[35] Takeishi, N. and Kawahara, Y. (2020). Learning dynamics models with stable invariant sets. In *AAAI Conference on Artificial Intelligence (AAAI)*.

[36] Teshima, T., Tojo, K., Ikeda, M., Ishikawa, I., and Oono, K. (2020). Universal Approximation Property of Neural Ordinary Differential Equations. In *NeurIPS Workshop on Differential Geometry meets Deep Learning (DiffGeo4DL)*.

[37] Wang, Q. (2013). Forward and adjoint sensitivity computation of chaotic dynamical systems. *Journal of Computational Physics*, 235:1–13.

[38] Yang, G., Huang, X., Hao, Z., Liu, M. Y., Belongie, S., and Hariharan, B. (2019). Pointflow: 3D point cloud generation with continuous normalizing flows. *International Conference on Computer Vision (ICCV)*, 2019-Octob:4540–4549.

[39] Zhuang, J., Dvornek, N., Li, X., Tatikonda, S., Papademetris, X., and Duncan, J. (2020). Adaptive Checkpoint Adjoint Method for Gradient Estimation in Neural ODE. In *International Conference on Machine Learning (ICML)*, number 1.

[40] Zhuang, J., Dvornek, N. C., Tatikonda, S., and Duncan, J. S. (2021). MALI: A memory efficient and reverse accurate integrator for Neural ODEs. (2020):1–22.

# Supplementary Material: Appendices

## A Derivation of Variational System

Let us consider a perturbed initial condition  $\bar{x}_0 = x_0 + \bar{\delta}_0$ , from which the solution  $\bar{x}(t)$  arises. Suppose that the solution  $\bar{x}(t)$  satisfies  $\bar{x}(t) = x(t) + \bar{\delta}(t)$ . Then,

$$\begin{aligned} \frac{d}{dt} \bar{\delta} &= \frac{d}{dt}(\bar{x} - x) \\ &= f(\bar{x}, t) - f(x, t) \\ &= \frac{\partial f}{\partial x}(x, t)(\bar{x} - x) + o(|\bar{x} - x|) \\ &= \frac{\partial f}{\partial x}(x, t)\bar{\delta} + o(|\bar{\delta}|), \\ \bar{\delta}(0) &= \bar{\delta}_0. \end{aligned} \tag{9}$$

Dividing  $\bar{\delta}$  by  $\bar{\delta}_0$  and taking the limit as  $|\bar{\delta}_0| \rightarrow +0$ , we define the variational variable as  $\delta(t) = \frac{\partial x(t)}{\partial x_0}$  and the *variational system* as

$$\frac{d}{dt} \delta(t) = \frac{\partial f}{\partial x}(x(t), t)\delta(t) \text{ for } \delta(0) = I. \tag{10}$$

## B Proofs

### Proof of Remark 1:

$$\frac{d}{dt}(\lambda^\top \delta) = \left(\frac{d}{dt}\lambda\right)^\top \delta + \lambda^\top \left(\frac{d}{dt}\delta\right) = \left(-\frac{\partial f}{\partial x}(x, t)^\top \lambda\right)^\top \delta + \lambda^\top \left(\frac{\partial f}{\partial x}(x, t)\delta\right) = 0. \tag{11}$$

**Proof of Remark 3:** Differentiating each term in the Runge-Kutta method in Eq. (5) by the initial condition  $x_0$  gives the Runge-Kutta method applied to the variational variable  $\delta$  as follows.

$$\begin{aligned} \delta_{n+1} &= \delta_n + h_n \sum_{i=1}^s b_i d_{n,i}, \\ d_{n,i} &:= \frac{\partial k_{n,i}}{\partial x_0} = \frac{\partial f(X_{n,i}, t_n + c_i h_n)}{\partial x_0} = \frac{\partial f(X_{n,i}, t_n + c_i h_n)}{\partial X_{n,i}} \Delta_{n,i}, \\ \Delta_{n,i} &:= \frac{\partial X_{n,i}}{\partial x_0} = \delta_n + h_n \sum_{j=1}^s a_{i,j} d_{n,j}. \end{aligned} \tag{12}$$

**Proof of Theorem 1:** Since the quantity  $S$  is conserved in continuous time,

$$\frac{d}{dt} S(\delta, \lambda) = 0. \tag{13}$$

Since the quantity  $S$  is bilinear,

$$\frac{d}{dt} S(\delta, \lambda) = \frac{\partial S}{\partial \delta} \frac{d\delta}{dt} + \frac{\partial S}{\partial \lambda} \frac{d\lambda}{dt} = S\left(\frac{d\delta}{dt}, \lambda\right) + S\left(\delta, \frac{d\lambda}{dt}\right), \tag{14}$$

which implies

$$S(d_{n,i}, \Lambda_{n,i}) + S(\Delta_{n,i}, l_{n,i}) = 0. \tag{15}$$

The change in the bilinear quantity  $S(\delta, \lambda)$  is

$$\begin{aligned}
S(\delta_{n+1}, \lambda_{n+1}) - S(\delta_n, \lambda_n) &= S(\delta_n + h_n \sum_i b_i d_{n,i}, \lambda_n + h_n \sum_i B_i l_{n,i}) - S(\delta_n, \lambda_n) \\
&= \sum_i b_i h_n S(d_{n,i}, \lambda_n) + \sum_i B_i h_n S(\delta_n, l_{n,i}) \\
&\quad + \sum_i \sum_j b_i B_j h_n^2 S(d_{n,i}, l_{n,j}) \\
&= \sum_i b_i h_n S(d_{n,i}, \Lambda_{n,i} - h_n \sum_j A_{i,j} l_{n,j}) \\
&\quad + \sum_i B_i h_n S(\Delta_{n,i} - h_n \sum_j a_{i,j} d_{n,j}, l_{n,i}) \\
&\quad + \sum_i \sum_j b_i B_j h_n^2 S(d_{n,i}, l_{n,j}) \\
&= \sum_i h_n (b_i S(d_{n,i}, \Lambda_{n,i}) + B_i S(\Delta_{n,i}, l_{n,i})) \\
&\quad + \sum_i \sum_j (-b_i A_{i,j} - B_j a_{j,i} + b_i B_j) h_n^2 S(d_{n,i}, l_{n,j}).
\end{aligned} \tag{16}$$

If  $B_i = b_i$  and  $b_i A_{i,j} + B_j a_{j,i} - b_i B_j = 0$ , the change vanishes, i.e., the partitioned Runge-Kutta conserves a bilinear quantity  $S$ . Note that  $A_{i,j} = B_j (1 - a_{j,i}/b_i)$  and hence  $b_i$  must not vanish. Hence, the bilinear quantity  $\lambda_n^\top \delta_n$  is conserved as

$$\lambda_N^\top \delta_N = \lambda_n^\top \delta_n \text{ for } n = 0, \dots, N. \tag{17}$$

By definition,  $\delta_n = \frac{\partial x_n}{\partial x_0}$ . When  $\lambda_N$  is set to  $\frac{\partial \mathcal{L}(x_N)}{\partial x_N}$ ,

$$\frac{\partial \mathcal{L}(x_N)}{\partial x_0} = \frac{\partial \mathcal{L}(x_N)}{\partial x_N} \frac{\partial x_N}{\partial x_0} = \lambda_N^\top \delta_N = \lambda_n^\top \delta_n = \frac{\partial \mathcal{L}(x_N)}{\partial x_n} \frac{\partial x_n}{\partial x_0}, \tag{18}$$

Therefore,  $\lambda_n = (\frac{\partial \mathcal{L}(x_N)}{\partial x_n})^\top$

**Proof of Theorem 2:** By solving the combination of the integrators in Eqs. (5) and (7), a change in a bilinear quantity  $S(\delta, \lambda)$  that the continuous-time dynamics conserves is

$$\begin{aligned}
S(\delta_{n+1}, \lambda_{n+1}) - S(\delta_n, \lambda_n) &= S(\delta_n + h_n \sum_i b_i d_{n,i}, \lambda_n + h_n \sum_i \tilde{b}_i l_{n,i}) - S(\delta_n, \lambda_n) \\
&= \sum_i b_i h_n S(d_{n,i}, \lambda_n) + \sum_i \tilde{b}_i h_n S(\delta_n, l_{n,i}) \\
&\quad + \sum_i \sum_j b_i \tilde{b}_j h_n^2 S(d_{n,i}, l_{n,j}) \\
&= \sum_{i \notin I_0} b_i h_n S(d_{n,i}, \Lambda_{n,i} - h_n \sum_j \tilde{b}_j (1 - a_{j,i}/b_i) l_{n,j}) \\
&\quad + \sum_i \tilde{b}_i h_n S(\Delta_{n,i} - h_n \sum_j a_{i,j} d_{n,j}, l_{n,i}) \\
&\quad + \sum_{i \notin I_0} \sum_j b_i \tilde{b}_j h_n^2 S(d_{n,i}, l_{n,j}) \\
&= \sum_{i \notin I_0} b_i h_n (S(d_{n,i}, \Lambda_{n,j}) + S(\Delta_{n,i}, l_{n,j})) \\
&\quad + \sum_{i \notin I_0} \sum_j (-b_i \tilde{b}_j (1 - a_{j,i}/b_i) - \tilde{b}_j a_{j,i} + b_i \tilde{b}_j) h_n^2 S(d_{n,i}, l_{n,j}) \\
&\quad + \sum_{i \in I_0} (\tilde{b}_i h_n S(\Delta_{n,i}, l_{n,j}) - \sum_j \tilde{b}_j a_{j,i} h_n^2 S(d_{n,i}, l_{n,j})) \\
&= \sum_{i \notin I_0} b_i h_n (S(d_{n,i}, \Lambda_{n,j}) + S(\Delta_{n,i}, l_{n,j})) \\
&\quad + \sum_{i \in I_0} h_n^2 (S(d_{n,i}, \Lambda_{n,j}) + S(\Delta_{n,i}, l_{n,j})) \\
&= 0.
\end{aligned} \tag{19}$$

Hence, the bilinear quantity  $S(\delta, \lambda)$  is conserved.

**Proof of Remark 4:** Eq. (6) is rewritten as

$$\begin{aligned}
\lambda_n &= \lambda_{n+1} - h_n \sum_{i=1}^s b_i l_{n,i} \\
l_{n,i} &= -\frac{\partial f}{\partial x}(X_{n,i}, t_n + c_i h_n)^\top \Lambda_{n,i}, \\
\Lambda_{n,i} &= \lambda_{n+1} - h_n \sum_{i=1}^s b_j \frac{a_{j,i}}{b_i} l_{n,j}.
\end{aligned} \tag{20}$$

Eq. (7) can be rewritten as

$$\begin{aligned}\lambda_n &= \lambda_{n+1} - h_n \sum_{i=1}^s \tilde{b}_i l_{n,i}, \\ l_{n,i} &= -\frac{\partial f}{\partial x}(X_{n,i}, t_n + c_i h_n)^\top \Lambda_{n,i}, \\ \Lambda_{n,i} &= \begin{cases} \lambda_{n+1} - h_n \sum_{j=1}^s \tilde{b}_j \frac{a_{j,i}}{\tilde{b}_i} l_{n,j} & \text{if } i \notin I_0 \\ -\sum_{j=1}^s \tilde{b}_j a_{j,i} l_{n,j} & \text{if } i \in I_0. \end{cases}\end{aligned}\quad (21)$$

Since  $a_{i,j} = 0$  for  $j \geq i$ ,  $a_{j,i} = 0$  for  $j \leq i$ . The intermediate adjoint variable  $\Lambda_{n,i}$  is calculable from  $i = s$  to  $i = 1$  sequentially, i.e., the integration backward in time is explicit.

## C Gradients in General Cases

**Gradient w.r.t. Parameters:** One can consider the parameters  $\theta$  as a part of the augmented state  $\tilde{x} = [x \ \theta]^\top$  of the system

$$\frac{d}{dt} \tilde{x} = \tilde{f}(\tilde{x}, t), \quad \tilde{f}(\tilde{x}, t) = \begin{bmatrix} f(x, t, \theta) \\ 0 \end{bmatrix}, \quad \tilde{x}(0) = \begin{bmatrix} x_0 \\ \theta \end{bmatrix}. \quad (22)$$

The variational system is also augmented in the same way. For the augmented adjoint variable  $\tilde{\lambda} = [\lambda \ \lambda_\theta]^\top$ , the adjoint system is

$$\frac{d}{dt} \tilde{\lambda} = -\frac{\partial \tilde{f}}{\partial \tilde{x}}(\tilde{x}, t)^\top \tilde{\lambda} = -\begin{bmatrix} \frac{\partial f}{\partial x}^\top & 0 \\ \frac{\partial f}{\partial \theta}^\top & 0 \end{bmatrix} \begin{bmatrix} \lambda \\ \lambda_\theta \end{bmatrix} = \begin{bmatrix} -\frac{\partial f}{\partial x}^\top \lambda \\ -\frac{\partial f}{\partial \theta}^\top \lambda \end{bmatrix}. \quad (23)$$

Hence, the adjoint variable  $\lambda$  for the system state  $x$  is unchanged from Eq. (3), and the one  $\lambda_\theta$  for the parameters  $\theta$  depends on the former as

$$\frac{d}{dt} \lambda_\theta = -\frac{\partial f}{\partial \theta}(x, t, \theta)^\top \lambda, \quad \lambda_\theta(T) = \frac{\partial \mathcal{L}(x(T), \theta(T))}{\partial \theta(T)}^\top, \quad (24)$$

and  $\lambda_\theta(0) = \frac{\partial \mathcal{L}(x(T), \theta)}{\partial \theta}^\top$ .

**Gradient of Functional:** When the solution  $x(t)$  is evaluated by a functional  $\mathcal{C}$  as

$$\mathcal{C}(x(t)) = \int_0^T \mathcal{L}(x(t), t) dt, \quad (25)$$

the adjoint variable  $\lambda_C$  that denotes the gradient  $\lambda_C(t) = \frac{\partial \mathcal{C}(x(T), t)}{\partial x(t)}$  of the functional  $\mathcal{C}$  is given by

$$\frac{d}{dt} \lambda_C = -\frac{\partial f}{\partial x}(x, t)^\top \lambda_C + \frac{\partial \mathcal{L}(x(t), t)}{\partial x(t)}, \quad \lambda_C(T) = \mathbf{0}. \quad (26)$$

## D Robustness to Rounding Error

By definition, the naive backpropagation algorithm, ANODE, ACA, and the proposed symplectic adjoint method provide the exact gradient up to rounding error. However, the naive backpropagation and ANODE obtained slightly worse results on GAS, POWER, and HEPMASS datasets. Due to the repeated use of the neural network, each method accumulates the gradient of the parameters  $\theta$  for each use. Let  $\theta_{n,i}$  denote the parameters used in  $i$ -th stage of  $n$ -th step even though their values are unchanged. The backpropagation algorithm obtains the gradient  $\frac{\partial \mathcal{L}}{\partial \theta}$  w.r.t. the parameters  $\theta$  by accumulating the gradient over all stages and steps one-by-one as

$$\frac{\partial \mathcal{L}}{\partial \theta} = \sum_{\substack{n=0, \dots, N-1, \\ i=1, \dots, s}} \frac{\partial \mathcal{L}}{\partial \theta_{n,i}}. \quad (27)$$

When step size  $h_n$  at  $n$ -th step is sufficiently small, the gradient  $\frac{\partial \mathcal{L}}{\partial \theta_{n,i}}$  at  $i$ -the stage may be insignificant compared to the accumulated gradient and be rounded off during the summation.

Conversely, the ACA accumulates the gradient within a step and then over time steps; this process can be expressed informally as

$$\frac{\partial \mathcal{L}}{\partial \theta} = \sum_{n=0}^{N-1} \left( \sum_{i=1}^s \frac{\partial \mathcal{L}}{\partial \theta_{n,i}} \right). \quad (28)$$

Also, according to Eqs. (6) and (24), the (symplectic) adjoint method accumulates the adjoint variable  $\lambda$  (i.e., the transpose of the gradient) within a step and then over time steps as

$$\lambda_{\theta,n} = \lambda_{\theta,n+1} - h_n \left( \sum_{i=1}^s B_i \left( -\frac{\partial f}{\partial \theta_{n,i}}(X_{n,i}, t + C_i h_n, \theta_{n,i})^\top \Lambda_{n,i} \right) \right). \quad (29)$$

In these cases, even when step size  $h_n$  at  $n$ -th step is small, the gradient summed within a step (over  $s$  stages) may be still significant and robust to a rounding error. This is why the adjoint method, ACA, and proposed symplectic adjoint method worked better than the naive backpropagation algorithm and ANODE for some datasets. Note that this approach needs additional memory footprint to store the gradient summed within a step, and it is applicable to the backpropagation algorithm by a slight modification.